Design of PrisMAV: An Omnidirectional Aerial Manipulator based on a 3-PUU Parallel Mechanism

Matthias Rubio, Joshua Näf, Franz Bühlmann, Philippe Brigger, Moritz Hüsser, Martin Inauen, Nicole Ospelt, Daniel Gisler, Marco Tognon, Roland Siegwart

Preprint version, final version at http://ieeexplore.ieee.org/ 2023 International Conference on Unmanned Aircraft Systems (ICUAS)

Design of *PrisMAV*: An Omnidirectional Aerial Manipulator based on a 3-PUU Parallel Mechanism

Matthias Rubio[1], Joshua Näf[1], Franz Bühlmann[1], Philippe Brigger[1], Moritz Hüsser[1], Martin Inauen[1], Nicole Ospelt[1], Daniel Gisler[1], Marco Tognon[1] and Roland Siegwart[1]

***Abstract*— The study of aerial robots capable to interact with their environment, also known as aerial manipulation, is a particularly new field in robotics research. Most existing solutions of aerial manipulators utilize commercially available multirotors as base flying platforms which are often extended by a suitable robotic arm. Although this design approach allows for fast prototyping, it impedes the development of a well-composed system where the base and the manipulator are designed conjointly. In contrast, this work presents a novel aerial manipulator featuring a 3-PUU (prismatic universal universal) parallel mechanism making up the structure of the flying platform. The key idea of using a parallel mechanism comes from its ability to quickly compensate positional errors of the platform while keeping the inertia of the moving parts low. To enable manipulation from any pose, *PrisMAV* is further designed to be omnidirectional by utilizing four tiltable rotor groups. The concept was successfully verified in a pick and place mission by grasping and releasing an object from above and from the side. The end-effector position tracking of *PrisMAV* is proven to be more accurate compared to a hypothetical fixed end-effector. The final result is a full proof of concept of an omnidirectional aerial manipulator.**

I. Introduction

Micro aerial vehicles (MAVs) have gained a significant amount of market traction for personal and industrial use over the last years. Still, active interaction with objects or pick & place missions have not yet gained a foothold in industry, even though such tasks are commonplace for ground robots. Due to the increased mechanical and dynamic complexity of aerial manipulators (AMs) compared to conventional MAVs, this topic has been limited to academic research [1], [2], [3]. Possible applications of AMs are vast, ranging from power line maintenance, over welding and contact-based inspection of pipes on a refinery [4], to collecting objects on inaccessible rooftops and construction work on skyscrapers. In the future, AMs could provide efficient and safe techniques to carry out general labour tasks in remote and dangerous locations.

As of today, many implementations of AMs consist of a quad- or hexarotor morphology with an attached manipulator [5], [6], [7], [8]. This approach benefits from the ability to reuse off-the-shelf multirotors and manipulators, which require less mechanical development and thus facilitate the entry to the field. Note that the need for a robotic arm is not strictly necessary to physically interact with the environment. Instead, zero degrees of freedom (DoF) end-effectors could be used which would reduce the weight and mechanical complexity of the manipulator. An example is demonstrated in [9], where they present different approaches of rigidly mounted grippers on a quadrotor platform for pick and transport missions. One downside of using a fixed end-effector is the loss of DoF which causes a decrease in the set of reachable grasping points around the platform's body. Depending on the application, the workspace of an AM is a crucial characteristic. In general, it is desired to maximize the workspace which can be achieved in different ways. One approach is presented in [10], where a quadrotor is equipped with a 2-DoF parallel manipulator to achieve an omnidirectional workspace.

Fig. 1. *PrisMAV*, the integrated aerial manipulator with a linear delta arm.

In contrast to increasing the DoF of the manipulator, the workspace can also be expanded by exploiting the maneuverability of the chosen floating base. More specifically, by using an omnidirectional platform [11]. The additional DoF required for omnidirectionality can be achieved by placing fixed thrust actuators in a specific way [12], [13] or by actuating the direction of the thrust axes with respect to the body by having tiltable propeller arms as shown in [14], [15]. Thereafter, the missing DoF incurred by using a fixed end-effector can be allocated on an omnidirectional platform to achieve the full 6-DoF. Nevertheless, a robotic arm can increase the AM's precision, since it can compensate for the slow flight dynamics.

It has to be mentioned that using a parallel manipulator can be advantageous since it generally has lower inertia and higher stiffness compared to a serial arm with equivalent DoF. The reason for this is that a parallel manipulator has

[1]Autonomous Systems Lab, Department of Mechanical Engineering, ETH Zürich, 8092 Zürich, Switzerland, mrubio@ethz.ch

its actuators located at the base rather than at each joint. Therefore, it can cover a higher bandwidth for error compensation while minimizing the resulting reaction forces on the floating base. The favourable weight distribution of a parallel manipulator also induces a reduction of the system's inertia which can increase the flying platform's agility. Additionally, a parallel manipulator is much less sensitive to errors in actuator position tracking compared to a serial manipulator, where the error is accumulated over all joints. This is also a desirable characteristic for high precision applications. A specific implementation of a parallel manipulator on an omnidirectional hexacopter was shown in [16].

This work aims to showcase a novel AM design which incorporates the previously mentioned advantages of a parallel mechanism with the desired agility of an omnidirectional floating base. Following a top-down design approach starting from the end-effector, the manipulator and the flying platform were developed conjointly resulting in a unified and fully integrated system design. The presented AM *PrisMAV* (see Figure 1), is based on tilting rotors and a delta manipulator with three limbs having prismatic-universal-universal (3-PUU) joints. Especially the linear delta manipulator is chosen due to its enclosing structure which allows the robotic arm to be fully retractable into the main body of the AM. This keeps the design compact and allows the platform to land on its main structure. In the context of pick and place missions, the platform can retract grasped objects into its body and protect them during flight, particularly when landing or taking off. Furthermore, the proposed omnidirectional base platform uses only 4 tilting rotor groups compared to six on an omnidirectional hexacopter. The advantage of using a parallel robotic arm is shown by comparing the position tracking performance to a hypothetical fixed end-effector in static hover mode. Additionally, the design was validated in experiments by performing pick and place missions by using an adaptive end-effector. One mission was performed such that the gripper is pointing downwards and another where it is pointing to the side. In both missions, an object was grasped from a static location and released at another position. Finally, the critical parts of the design and possible improvements, as well as the impact on future applications in the field are discussed.

II. Hardware Design

The focus of *PrisMAV* is to perform pick and place missions because this implies general tasks such as grasping an object and transporting it over small distances. For the missions, the test object to manipulate was defined as an aluminum cylinder of $0.5\,\mathrm{kg}$ with a diameter of $8\,\mathrm{cm}$ and a height of $20\,\mathrm{cm}$. An example of an actual pick and place mission can be the positioning of delicate sensors in high or inaccessible areas on industrial sites. To achieve those tasks, the system has to be able to interact precisely with the object during the grasping and placing maneuvers. By analyzing the positional error data of an existing omnidirectional MAV [15], the necessary workspace of the AM can be estimated. A spectral analysis of the positional error from the existing platform shows that a maximum error amplitude of $4\,\mathrm{cm}$ is reached at a frequency of approximately $1\,\mathrm{Hz}$. To compensate this positional error including an additional safety margin, the manipulator workspace should be designed to cover a cylindrical workspace with a radius of $5.6\,\mathrm{cm}$ and a depth of $10\,\mathrm{cm}$. Furthermore the end-effector should achieve omnidirectionality to be able to pick and place the object in any given orientation. In the following subsections we present the design procedure starting from choosing the appropriate end-effector up to composing the complete AM *PrisMAV*, which can be seen in Figure 1.

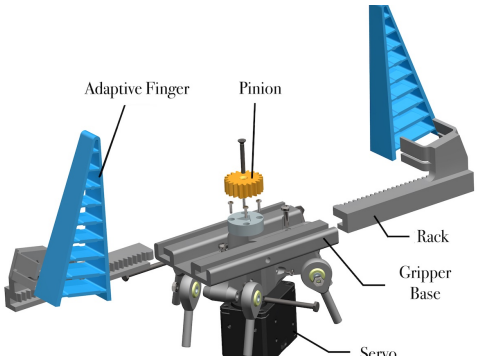

Fig. 2. Explosion view of the end-effector assembly.

A. End-Effector

To grasp objects of varying sizes and geometries, we equip *PrisMAV* with commercial adaptive fingers. To actuate them, a rack and pinion-based mechanism is used thanks to its low complexity and high actuation speeds, which are beneficial when trying to grasp an object in flight. An explosion view of the model can be seen in Figure 2. The mechanism is actuated by a servo motor which is recessed into the gripper base which connects the manipulator linkages and the end-effector. The servo itself is rigidly mounted into the gripper base and hence serves as additional structural support. For the racks and the pinion, a light-weight and wear-resistant plastic is used. To increase the grip of the adaptive fingers on smooth materials they are coated by a layer of silicone on their contact surfaces. This reduces the necessary torque that the servo needs to produce when grasping an object. The minimum opening width is set to be at least $10\,\mathrm{cm}$ for the cylinder of $8\,\mathrm{cm}$ in diameter in order to account for uncertainties in the error compensation of the manipulator.

B. Manipulator as Base Structure

To be able to compensate the expected positional error of the platform, a parallel manipulator is chosen due to its fast dynamics and centralized weight distribution which leads to an overall lower inertia of the platform. Specifically, a 3-PUU linear delta manipulator is selected, which was highly inspired by similarly constructed 3D-printers. The ability of those printers to perform their desired tasks uniquely inside their structure was a key feature in the decision process. Their outer structure could be used as the body of

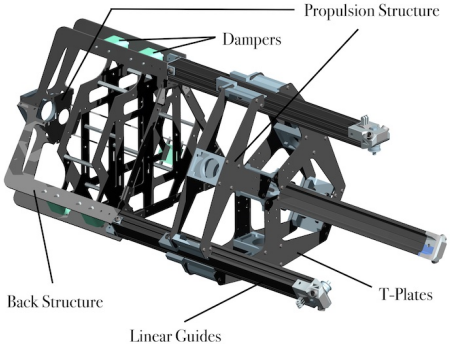

Fig. 3. The main body structure of *PrisMAV*.

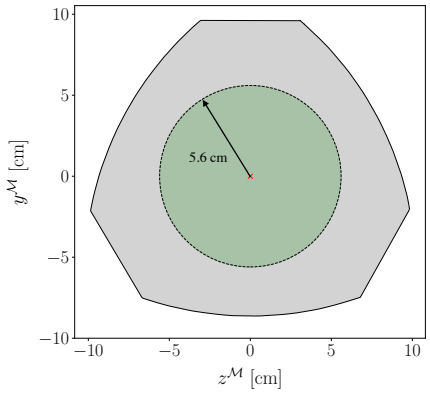

Fig. 4. Workspace of the manipulator (grey) and the desired compensation capability (green) as seen from the front view (gripping direction).

Component	Name
On-Board Computer	Up Board Xtreme i7
Propulsion Motor	MAD 5008 EEE 400KV
ESC	Holybro Kotleta20
Tilt/Gripper Motor	Dynamixel XL430-W250-T
Arm Motor	Maxon ECXTQ22M
DC Driver	Trinamic TMCM-1640
IMU	VectorNav VN-100
Battery	Swaytronic LiPo 6S 6200 mAh

TABLE I

OVERVIEW OF THE ELECTRICAL COMPONENTS AND ACTUATORS.

the whole AM, setting the design apart from the state-of-the-art approach of composing an existing flying platform with a manipulator. Furthermore, the manipulator and the object can be easily retracted into the structure providing a protective enclosure for delicate objects, such as sensors or expensive tools. One can even think of performing some task on the object inside the structure during the transportation from one location to another, e.g., by evaluating a collected ground sample by using spectroscopy or a computer vision algorithm to analyze the composition of the collected sample. In future applications, this could reduce the number of flights necessary to gather the desired information and hence the overall mission time. In our case, having a fully retractable manipulator makes the design more compact and it enables *PrisMAV* to land on its structure, as all the other faces of the AM are obstructed by propellers.

The base structure consists of three carbon linear guides for the manipulator, giving the system the shape of a triangular prism. To hold the linear guides in place and to rigidly attach the rotor groups to the system, T-shaped carbon plates are used which are connected together by aluminum parts as shown in Figure 3. This rigid arrangement prevents the guides from bending and facilitates precise operation of the manipulator during interaction. The manipulator is actuated by three brushless DC motors located at the end of the linear guides. The rotational motion is translated into linear motion via a toothed belt drive. The belts are attached to three low friction polymer sliders gliding along the carbon linear guides. The 3D-printed end-effector base is then connected to the sliders using three linkages each made up of two carbon tubes and bilaterally ending on ball joints. The dimensions for the arm linkages and the linear guides are chosen such that i) the manipulator is fully retractable into the prismatic structure, ii) the end-effector extension is at least $10\,\mathrm{cm}$ outside of the surrounding structure, and iii) the required workspace can be fully covered. As visualized in Figure 4, the workspace computed with the dimensions of the actual manipulator exceeds the required workspace.

C. Electronics

The electronic components are located on the back plate, which houses batteries, the IMU and the integrated computer which features an Intel core i7 and an STM32 micro controller. The on-board computer can be accessed through a Wi-Fi connection from a remote operator. Damping elements made out of silicone decouple the back plate from the rest of the system. Making use of the high inertia of the batteries, this damping method attenuates high frequency vibrations generated by the actuators of *PrisMAV* which would negatively affect IMU measurements and may strain and damage the electronic components in the long term. The electronic speed controllers for the thrust generating actuators are connected to the computer via a CAN bus interface. The power for the whole system comes from two $6200\,\mathrm{mAh}$ batteries at $22\,\mathrm{V}$ which provide an estimated mean flight time of $10\,\mathrm{min}$ in hover mode. Table I gives an brief overview of the electrical components and actuators used on *PrisMAV*.

D. Towards an Aerial Manipulator

The platform features four rotor arms allocated at the vertices of a tetrahedron, each carrying a propeller group which can tilt around its respective axis (see Figure 1). Note that this arrangement together with the extended delta arm ensures a safe distance to the operating point at the end-effector to prevent possible collisions of the propellers or the structure with the environment. A possible scenario could be *PrisMAV* bringing a tool to a human construction worker who is operating at height, where a safety margin is crucial. To increase the thrust and to cancel out the drag torque, each propeller group consists of two coaxial, counter-rotating rotors and is able to exert a maximum thrust force of $40\,\mathrm{N}$.

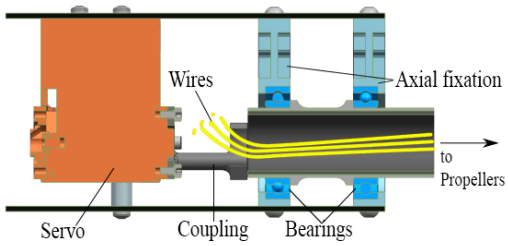

Fig. 5. Section view of the tilt mechanism.

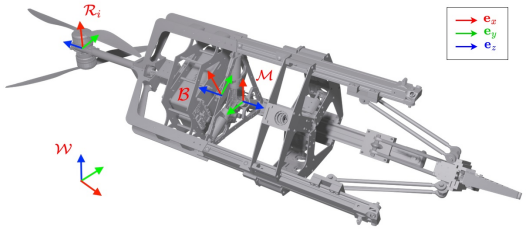

Fig. 6. Coordinate frames used for system modeling and control.

The tilting mechanism of the rotor groups is actuated by servo motors as can be seen in detail in Figure 5. The wiring for the propellers yields enough slack to allow for up to two full rotations in both directions, making almost any maneuver possible. The design of the tilt mechanism and the propeller group arrangement was inspired by existing platforms such as the one demonstrated in [17]. In contrast to this platform, our system involves an additional tiltable propeller group, leading to three propeller groups in the front. This extra propeller group enables *PrisMAV* to also rotate around its roll axis (i.e., the direction of the end-effector), granting the desired six degrees of freedom and hence omnidirectional flight and manipulation.

Summarizing the hardware design, *PrisMAV* is composed of a 3-PUU delta manipulator to compensate for the positional inaccuracies of the flying platform. An adaptive gripper is used as the end-effector, which enables manipulation of variously shaped objects in the context of pick and place missions. To make the system fly omnidirectionally, four tiltable propeller groups are placed at the vertices of a tetrahedron. This allows the AM, and hence the end-effector to hover in any arbitrary orientation in space. The final design of *PrisMAV* has a diameter of about $0.95\,\mathrm{m}$ while being $1.33\,\mathrm{m}$ tall. Furthermore, the prototype weighs approximately $7.7\,\mathrm{kg}$.

III. System Modeling

To allow for decoupled development and testing, the model is split into two separate subsystems: the flying platform and the manipulator. In the following, it is assumed that the bodies are rigid and that no mechanical play or friction is present in the moving parts.

A. Coordinate Frames

To describe the full configuration of the platform in the inertial frame $\mathcal{W}$, a body-fixed, a manipulator and a rotor coordinate frame are introduced (see Figure 6). The body-fixed frame $\mathcal{B}$ is located at the IMU and aligned accordingly. The manipulator frame $\mathcal{M}$ is placed at the geometric center of the equilateral triangle spanned by the three linear guides. Its z-axis is parallel to the linear guides and the origin of its z-coordinate is at the height of the sliders when they are fully retracted into the structure. The four rotor frames $\mathcal{R}_i$, $i \in \{1,2,3,4\}$ are attached to the rotor groups, where the x-axis is coincident with the corresponding thrust vector and the z-axis of the rotor frame is centered in the corresponding carbon tube.

B. Aerodynamics and Allocation

A simplified aerodynamic model is introduced where we assume a quadratic relationship between the force $\mathbf{f}_i \in \mathbb{R}^3$ and drag torque $\boldsymbol{\tau}_i \in \mathbb{R}^3$ produced by the i-th rotor group and its angular velocity ω.

$$\mathbf{f}_i^{\mathcal{R}_i} = \mu\omega_i^2\mathbf{e}_x^{\mathcal{R}_i} \qquad \boldsymbol{\tau}_i^{\mathcal{R}_i} = \kappa\omega_i^2\mathbf{e}_x^{\mathcal{R}_i}, \qquad i \in \{1,2,3,4\} \quad (1)$$

where μ is the thrust coefficient and κ is the drag torque coefficient of a propeller group. They can be derived empirically by conducting appropriate thrust tests. According to the previously introduced convention, $\mathbf{e}_x^{\mathcal{R}_i}$ denotes the thrust direction expressed in $\mathcal{R}_i$. The allocation matrix is formulated as proposed in [14] and [15]. Due to the co-axial propeller configuration the single rotor drag torques cancel each other out ($\kappa = 0$) and the following equations hold:

$$\mathbf{f}^{\mathcal{B}} = \sum_i \mathbf{f}_i^{\mathcal{B}} = \sum_i \mathbf{R}_{\mathcal{B}\mathcal{R}_i}\mathbf{f}_i^{\mathcal{R}_i} \quad (2)$$

$$\boldsymbol{\tau}^{\mathcal{B}} = \underbrace{\sum_i \boldsymbol{\tau}_i^{\mathcal{B}}}_{=0} + \sum_i \boldsymbol{\tau}_{\mathbf{f}_i^{\mathcal{B}}}^{\mathcal{B}} = \sum_i \mathbf{r}_i^{\mathcal{B}} \times \mathbf{f}_i^{\mathcal{B}} \quad (3)$$

where $\mathbf{R}_{\mathcal{B}\mathcal{R}_i}$ denotes the rotation matrix from the rotor coordinate frame $\mathcal{R}_i$ to the body fixed frame $\mathcal{B}$ and $\mathbf{r}_i^{\mathcal{B}}$ is the position of the i-th rotor group in $\mathcal{B}$. The equations can be formulated as a matrix-vector equation which results in:

$$\mathbf{w} = \begin{bmatrix}\mathbf{f}\\ \boldsymbol{\tau}\end{bmatrix}_{\mathcal{B}} = \mathbf{A}(\boldsymbol{\alpha})\begin{bmatrix}\hat{f}_1\\ \vdots\\ \hat{f}_4\end{bmatrix} = \mathbf{A}(\boldsymbol{\alpha})\hat{\mathbf{f}} \quad (4)$$

$$\hat{f}_i = \mu \cdot \omega_i^2 \qquad \forall i \in \{1,2,3,4\} \quad (5)$$

where $\mathbf{A}(\boldsymbol{\alpha}) \in \mathbb{R}^{6\times 4}$ is the angle dependent allocation matrix and $\mathbf{w} \in \mathbb{R}^6$ denotes the desired wrench. $\boldsymbol{\alpha}$ is defined as the vector containing all α_i which denote the rotation of the i-th rotor group around $\mathbf{e}_z^{\mathcal{R}_i}$. Due to the a priori unknown and variable tilt angles $\boldsymbol{\alpha}$, the allocation matrix is non-constant. Thus, the auxiliary variables u_k for $k \in \{1,2,\ldots,8\}$ are defined which eliminate the angle dependency of $\mathbf{A}(\boldsymbol{\alpha})$ and provide a constant allocation matrix $\hat{\mathbf{A}} \in \mathbb{R}^{6\times 8}$.

$$u_k = \begin{cases}\sin\left(\alpha_{k/2}\right)\cdot\mu\cdot\omega_{k/2}^2 & \text{if } k \text{ odd}\\ \cos\left(\alpha_{\lfloor k/2\rfloor}\right)\cdot\mu\cdot\omega_{\lfloor k/2\rfloor}^2 & \text{if } k \text{ even}\end{cases} \quad (6)$$

The auxiliary variables $\mathbf{u} = \begin{bmatrix}u_1 & \ldots & u_8\end{bmatrix} \in \mathbb{R}^8$ can then be calculated by:

$$\mathbf{u} = \hat{\mathbf{A}}^{+}\mathbf{w} \quad (7)$$

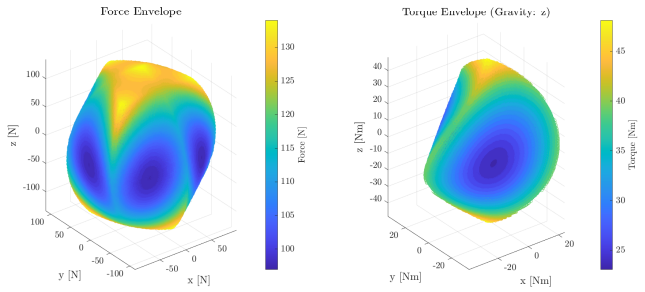

Fig. 7. Force and torque envelopes of *PrisMAV*. Most thrust is available in tricopter configuration (yellow areas), least thrust in horizontal configuration (blue areas).

It can be shown that the resulting constant allocation matrix with the given the system dimensions, has full row rank, $\operatorname{rank}\left(\hat{\mathbf{A}}\right) = 6$. Hence, *PrisMAV* is capable of exciting each dimension of the wrench-space independently with the proposed propeller allocation. The auxiliary variables $\mathbf{u}$ can then be transformed back to the desired tilt angles and rotor velocities by the use of trigonometric identities and the empirically obtained thrust coefficient μ.

$$\alpha_i = \operatorname{atan2}(u_{2i-1}, u_{2i}) \tag{8}$$

$$f_i = \sqrt{u_{2i-1}^2 + u_{2i}^2} \qquad \forall i \in \{1,2,3,4\} \tag{9}$$

$$\omega_i = \sqrt{\frac{f_i}{\mu}} \tag{10}$$

To examine the omnidirectionality and the possible configurations of *PrisMAV*, in Figure 7 we show the thrust and torque envelope of the platform. The thrust envelope demonstrates the maximum thrust which can be achieved along any direction by constraining the overall torque to zero. The torque envelope denotes the torque that can be achieved by the AM subject to the constraint of a static hover thrust along the body z-axis. The envelopes in Figure 7 show that the platform can exert sufficient amounts of force or torque in any arbitrary direction while compensating for gravity to achieve omnidirectional flight and manipulation. However, there are configurations with higher maximal thrust or torque magnitudes. For instance, approximately 1.4 times more thrust can be exerted in *tricopter configuration* (body z-axis is aligned with gravity, i.e., the end-effector pointing towards the floor or the ceiling) compared to *horizontal mode* (the body z-axis is normal to gravity, i.e., *PrisMAV* is pitched by $90°$).

It has to be mentioned that in certain orientations the AM finds itself in a singular configuration. For instance when the AM is flying in the tricopter configuration the top propeller servo angle is not uniquely defined as it is not needed for flight. A workaround to this issue is using an alternate allocation, where the propeller group in the singular configuration is not included. Nevertheless, in practice a low but non-zero RPM command is set to the top propeller to enable faster transition between the alternate and the regular allocation.

C. Rigid Body Dynamics

The equations of motion of the flying platform can be derived using the Newton-Euler equations as proposed in [15]. The resulting rigid body dynamics can be written as:

$$\mathbf{w} = \begin{bmatrix} m\mathbf{I}_3 & 0 \\ 0 & \mathbf{J}_{\text{AM}}^{\mathcal{B}} \end{bmatrix} \begin{bmatrix} \ddot{\mathbf{p}} \\ \dot{\boldsymbol{\omega}} \end{bmatrix}_{\mathcal{B}} + \begin{bmatrix} \boldsymbol{\omega} \times m\dot{\mathbf{p}} \\ \boldsymbol{\omega} \times \mathbf{J}_{\text{AM}}^{\mathcal{B}}\boldsymbol{\omega} \end{bmatrix}_{\mathcal{B}}, \tag{11}$$

where $\mathbf{I}_3$ is the 3×3 identity matrix, $\mathbf{J}_{\text{AM}}^{\mathcal{B}}$ denotes the moment of inertia in the body-fixed frame $\mathcal{B}$, $\mathbf{p}$, $\dot{\mathbf{p}}$, $\ddot{\mathbf{p}}$ denote the position, velocity and acceleration and $\boldsymbol{\omega}$, $\dot{\boldsymbol{\omega}}$ the angular velocity and angular acceleration of $\mathcal{B}$, i.e. the flying platform.

Due to the moving arm and the grasped object, the inertia $\mathbf{J}_{\text{AM}}^{\mathcal{B}}$ and mass m of the system are not constant. This implies that the center of mass (CoM) is changing over time, resulting in an offset $\mathbf{x}_{\text{com}}^{\mathcal{B}}$ from the body-fixed frame origin to the true CoM. In the nominal case, where the arm is fully retracted and no object is grasped, the nominal inertia $\mathbf{J}_{\text{AM,nm}}^{\mathcal{B}}$ and CoM were identified with the CAD model of the platform. Using the parallel axis theorem, a change in inertia is characterized by:

$$\begin{aligned} \mathbf{J}_{\text{AM}}^{\mathcal{B}} &= \mathbf{J}_{\text{AM,nm}}^{\mathcal{B}} + m \cdot \mathbf{D}, \\ \mathbf{D} &= \begin{bmatrix} y_m^2 + z_m^2 & -x_m y_m & -x_m z_m \\ -x_m y_m & x_m^2 + z_m^2 & -y_m z_m \\ -x_m z_m & -y_m z_m & x_m^2 + y_m^2 \end{bmatrix} \end{aligned} \tag{12}$$

where m is the mass being moved away from the nominal CoM and x_m, y_m, z_m are the corresponding displacements in the body-fixed frame $\mathcal{B}$, which can be compactly written in the form of a displacement matrix $\mathbf{D}$.

To model the change in inertia for *PrisMAV*, the sliders and end-effector assembly are assumed to be point masses, while the masses of the carbon tubes are neglected. Consequently the change of inertia equals to:

$$\mathbf{J}_{\text{AM}}^{\mathcal{B}} = \mathbf{J}_{\text{AM,nm}}^{\mathcal{B}} + m_{\text{slider}} \cdot \mathbf{D}_{\text{slider}} + m_{\text{ee}} \cdot \mathbf{D}_{\text{ee}}, \tag{13}$$

where $\mathbf{D}_{\text{slider}}$ is the displacement matrix for the sliders while $\mathbf{D}_{\text{ee}}$ is the displacement matrix for the end-effector. They can be calculated by comparing the current end-effector position with the fully retracted end-effector position.

D. Manipulator Kinematics

The inverse kinematics for a 3-PUU delta arm are derived analytically by formulating a closed loop vector equation as shown in Figure 8. The position of the end-effector $\mathbf{p}_{ee}^{\mathcal{M}} = \begin{bmatrix} x_{\text{ee}}^{\mathcal{M}} & y_{\text{ee}}^{\mathcal{M}} & z_{\text{ee}}^{\mathcal{M}} \end{bmatrix}^\top$ can be related to the joint positions $\mathbf{q} = \begin{bmatrix} q_1 & q_2 & q_3 \end{bmatrix}^\top$ as:

$$\mathbf{p}_{ee}^{\mathcal{M}} = \mathbf{R}_j + q_j \mathbf{e}_z + \mathbf{h}_j + \mathbf{d}_j + \mathbf{r}_j \qquad j \in \{1,\,2,\,3\} \tag{14}$$

Resolving (14) for q_j and taking the euclidean norm on both sides leads to the following equation:

$$q_j = f_j(\mathbf{p}_{ee}^{\mathcal{M}}) = z_{\text{ee}}^{\mathcal{M}} + \sqrt{d^2 - \left(x_{\text{ee}}^{\mathcal{M}} - E_j\right)^2 - \left(y_{\text{ee}}^{\mathcal{M}} - F_j\right)^2} \tag{15}$$

$$E_j := (R - h - r)\cos\varphi_j \qquad \forall j \in \{1,2,3\} \tag{16}$$

$$F_j := (R - h - r)\sin\varphi_j \tag{17}$$

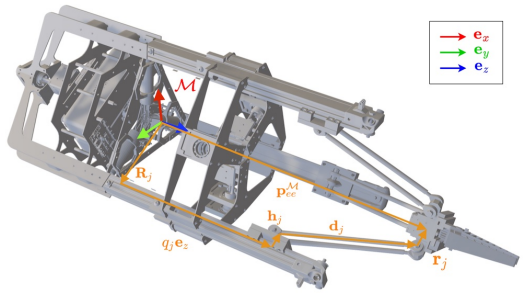

Fig. 8. Closed loop vector formulation for manipulator kinematics.

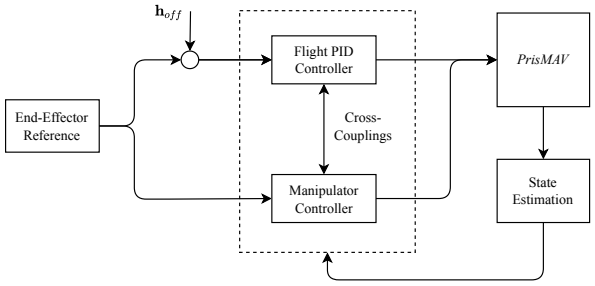

Fig. 9. Block diagram of the control structure adopted on the platform.

where $\varphi_j \in [0°, 240°, 120°]$ indicate the angles between $\mathbf{e}_x^{\mathcal{M}}$ and the linear guide with index j. R, h and r represent the magnitude of the corresponding vectors. Furthermore, the transform of the joint position q_j to the actuator angle θ_j with a radius r_{pulley} to the pulley belt is:

$$\theta_j = \frac{q_j}{r_{\text{pulley}}}. \tag{18}$$

The inverse Jacobian mapping $\mathbf{J}^{-1}(\mathbf{p}_{ee}^{\mathcal{M}})$ relating the end-effector velocity $\dot{\mathbf{p}}_{ee}^{\mathcal{M}}$ to the joint velocities $\dot{\mathbf{q}}$ is determined by analyzing the time derivative of $\mathbf{q} = \boldsymbol{f}(\mathbf{p}_{ee}^{\mathcal{M}})$.

$$\dot{\mathbf{q}} = \frac{\mathrm{d}\boldsymbol{f}(\mathbf{p}_{ee}^{\mathcal{M}})}{\mathrm{d}t} = \frac{\partial \boldsymbol{f}(\mathbf{p}_{ee}^{\mathcal{M}})}{\partial \mathbf{p}_{ee}^{\mathcal{M}}} \frac{\mathrm{d}\mathbf{p}_{ee}^{\mathcal{M}}}{\mathrm{d}t} =: \mathbf{J}^{-1}(\mathbf{p}_{ee}^{\mathcal{M}}) \dot{\mathbf{p}}_{ee}^{\mathcal{M}} \tag{19}$$

IV. Control

The control of the platform is split up into a flight controller and a manipulator controller (see Figure 9). This approach allowed disjoint development and testing of the two systems. Nevertheless, the influence of the manipulator motion on the flight controller (and vice-versa) is partially captured by adapting the CoM continuously as in (13).

The setpoints for each controller are obtained by specifying a desired (denoted with a top bar) pose for the end-effector in the world frame, i.e., a position $\bar{\mathbf{p}}_{ee}^{\mathcal{W}}$ and a rotation $\bar{\phi}_{ee}^{\mathcal{W}}$ described in Euler angles. The position setpoint for the flying platform $\bar{\mathbf{p}}^{\mathcal{W}}$ is computed by a static offset $\mathbf{h}_{off}$ from the desired end-effector position such that when the arm is extended the sliders should be at 75% of their way out (as in Figure 8). The desired rotation for the flying platform is the same as $\bar{\phi}_{ee}^{\mathcal{W}}$ since the parallel manipulator possesses only translational degrees of freedom. The position setpoint for the manipulator controller $\bar{\mathbf{p}}_{ee}^{\mathcal{M}}$ is computed by a coordinate transformation of $\bar{\mathbf{p}}_{ee}^{\mathcal{W}}$ to the manipulator frame. Note that this transformation depends on the current position and orientation of the flying platform.

A. Flight Controller

Using the equations of motion formulated in (III-C), a PID controller for the flying platform can be formulated as in (22) and (23), where the desired forces $\mathbf{f}_d$ and torques $\boldsymbol{\tau}_d$ are expressed in the body-fixed frame $\mathcal{B}$.

$$\mathbf{e}_{trans} = (-k_p\mathbf{e}_p - k_v\mathbf{e}_v - k_{pi}\mathbf{e}_{pi} + \ddot{\bar{\mathbf{p}}} + \mathbf{g}) \tag{20}$$

$$\mathbf{e}_{rot} = (-k_R\mathbf{e}_R - k_\omega\mathbf{e}_\omega - k_{Ri}\mathbf{e}_{Ri}) \tag{21}$$

$$\mathbf{f}_d = m(\mathbf{R}_{\mathcal{BW}}^\top \mathbf{e}_{trans} + (\boldsymbol{\omega}^{\mathcal{B}} \times \mathbf{R}_{\mathcal{BW}}^\top \dot{\mathbf{p}}^{\mathcal{B}})) \tag{22}$$

$$\boldsymbol{\tau}_d = \mathbf{J}_{\text{AM}}^{B}\mathbf{e}_{rot} + (\boldsymbol{\omega}^{\mathcal{B}} \times \mathbf{J}_{\text{AM}}^{\mathcal{B}}\boldsymbol{\omega}^{\mathcal{B}}) + (\mathbf{x}_{\text{com}}^{\mathcal{B}} \times \mathbf{f}_d) \tag{23}$$

where $\mathbf{R}_{\mathcal{BW}}$ is the rotation matrix from the inertial world frame $\mathcal{W}$ to the body-fixed frame $\mathcal{B}$, $\mathbf{g}$ the gravity vector along the inertial z-axis, m the mass of the platform, $\mathbf{J}_{\text{AM}}^{\mathcal{B}}$ the inertia, $\boldsymbol{\omega}^{\mathcal{B}}$ the angular velocity vector, $\ddot{\bar{\mathbf{p}}}$ the desired acceleration and $\dot{\mathbf{p}}^{\mathcal{B}}$ the velocity of the flying platform. The constants k_p, k_v, k_R and k_ω are the gains on position, velocity, rotation and angular rate errors. To eliminate a static lag error, integral terms on the position and rotation error are added and multiplied by the gains k_{pi} and k_{Ri}, respectively. The error terms $\mathbf{e}_p$, $\mathbf{e}_v$, $\mathbf{e}_R$ and $\mathbf{e}_\omega$ for position, velocity, orientation and angular velocity as well as the integrated error terms $\mathbf{e}_{pi}$ and $\mathbf{e}_{Ri}$ for position and rotation are calculated as proposed in [14].

B. Manipulator Controller

To control the delta manipulator such that the platform's positional error can be rejected, an inverse differential kinematic controller is proposed as follows:

$$\dot{\mathbf{q}} = \underbrace{\mathbf{J}^{-1}\left(\mathbf{p}_{ee}^{\mathcal{M}}\right)\dot{\bar{\mathbf{p}}}_{ee}^{\mathcal{M}}}_{\text{FF}} + \underbrace{k_{\text{P}} \cdot \mathbf{e}_{\text{q}} + k_{\text{I}} \cdot \int \mathbf{e}_{\text{q}}\,\mathrm{d}t + k_{\text{D}} \cdot \frac{\mathrm{d}\mathbf{e}_{\text{q}}}{\mathrm{d}t}}_{\text{PID}} \tag{24}$$

where $\mathbf{e}_{\text{q}} = \bar{\mathbf{q}} - \mathbf{q}$ and $\mathbf{J}^{-1}\left(\mathbf{p}_{ee}^{\mathcal{M}}\right)$ denotes the inverse Jacobian of the manipulator evaluated at the current end-effector position $\mathbf{p}_{ee}^{\mathcal{M}}$. The desired slider setpoints $\bar{\mathbf{q}}$ can be computed using (15) and the desired end-effector position $\bar{\mathbf{p}}_{ee}^{\mathcal{M}}$. Note that the desired velocity $\dot{\bar{\mathbf{p}}}_{ee}^{\mathcal{M}}$ is computed using finite differences. The actual slider positions $\mathbf{q}$ are obtained from the motor controllers (DC drivers) and close the feedback loop. It can be seen that the control law is split into a feedforward (FF) and a PID action. The FF action anticipates further changes in the setpoint while the PID control action enables offset-free tracking.

V. Results

The design was validated by testing it in an indoor environment. For these tests, an external motion tracking system

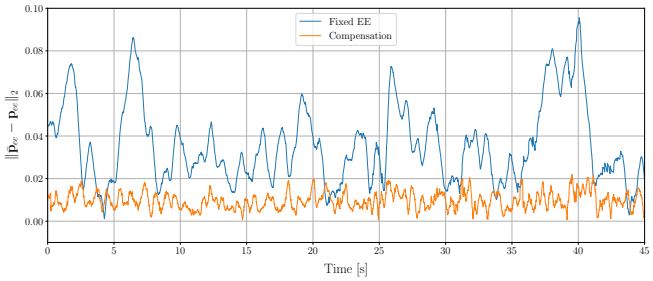

Fig. 10. Absolute positional error of a hypothetical fixed end-effector compared to the compensating delta arm. $\bar{\mathbf{p}}_{ee}$ and $\mathbf{p}_{ee}$ denote the desired and the actual end-effector position respectively.

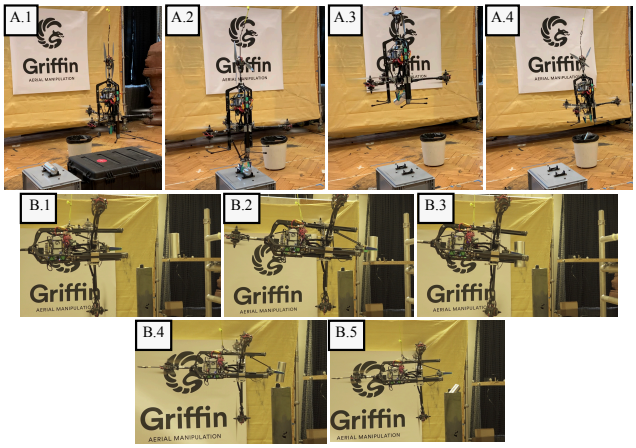

Fig. 11. Aerial manipulation missions in tricopter (A) and horizontal (B) configuration. A.1 Approach object. A.2 Grasp object. A.3 Retract arm. A.4 Place object. B.1 Approach object. B.2 Grasp object. B.3 Retract arm. B.4 Approach drop-off. B.5 Place object.

was used to perform the state estimation of the platform. The motion tracking system runs at 100 Hz whereas the on-board IMU runs at 300 Hz. The pose of the platform is estimated by feeding both measurements into a multi sensor fusion framework [18] based on an extended Kalman filter. The AM was tethered to a safety rope during all the flight and manipulation tests to reduce the risk of damaging the AM. Since the safety rope was loosely attached, it had only a minimal influence on the results.

To quantify the enhanced precision of the delta arm, the error of the end-effector with compensation is compared to the error of a hypothetical fixed end-effector in Figure 10. During the test, the platform was in its tricopter configuration (i.e. the end-effector pointing downwards) and a trajectory was followed along the gripping direction. One can see that the system with compensation has a significantly lower upper bound on the absolute error compared to the fixed end-effector. In particular note that when the fixed end-effector experienced large disturbances the compensating arm showed the desired behaviour of filtering out these large deviations.

Pick and place missions in the tricopter and horizontal configuration demonstrate the AM's general capabilities to interact with the environment (see Figure 11). For the tricopter mission (A), *PrisMAV* took off from a box. After approaching the object, the manipulator started to compensate the positional error of the flying platform. The delta arm moved out of the drone structure and grasped the object. After a successful grasp, the arm was retracted back into the platform structure with the grasped object and stopped compensating. Finally *PrisMAV* flew to the desired drop-off location, where the object was dropped into a basket.

The mission procedure for the horizontal configuration (B) is similar as for the tricopter mission except that the MAV started in a horizontal position.

VI. Discussion

This work presents *PrisMAV*, a novel aerial manipulator platform designed to perform pick and place missions. *PrisMAV* shows the advantages of using a parallel manipulator and exploits the maneuverability of the platform by using tilting rotor groups.

Especially, the system was designed such that the manipulator structure directly makes up the main body of the flying platform. This sets our platform apart from state-of-the-art aerial manipulators which generally piece together a flying base platform and a robotic arm. Furthermore, it was shown that integrating a parallel mechanism into a flying platform improves precision compared to using a fixed end-effector, enabling precise interaction of the platform with its environment. Pick and place missions were executed in two different flight modes to show the capability of manipulating in different orientations. Still, a critical part is to reduce the mass of the platform and increase its compactness. One could think of integrating the electronics on the side of the linear guides to reduce the overall size of the structure instead of placing them on the back plate which lies behind the manipulator. On the software side, more sophisticated and combined control strategies could be developed such as full-body control approaches or MPC-based control strategies which would include the dynamics of the manipulator. These more sophisticated control policies could lead to increased robustness of the platform in nominal flight, as well as close to singular configurations which could be avoided automatically. This increased robustness would also allow to remove the safety tether and the external motion tracking to perform extensive testing of pose transitions in realistic pick and place missions. The development of *PrisMAV* should contribute to aerial manipulation research by adding a new perspective on the composition of functionalities in the design process and should motivate the community to engineer unseen aerial manipulator designs.

Acknowledgment

The authors would like to thank Prof. Dr. Roland Siegwart, Dr. Marco Tognon, Dr. Jen Jen Chung, Michael Pantic, Julian Förster, Andreas Voigt, Karen Bodie and the ASL Staff for the valuable feedback and support during the project.

REFERENCES

[1] A. Ollero, M. Tognon, A. Suarez, D. Lee, and A. Franchi, "Past, present, and future of aerial robotic manipulators," *IEEE Transactions on Robotics*, vol. PP, pp. 1–20, 06 2021.

[2] X. Meng, Y. He, and J. Han, "Survey on aerial manipulator: System, modeling, and control," *Robotica*, vol. 38, no. 7, p. 1288–1317, 2020.

[3] M. Orsag, C. Korpela, P. Oh, and S. Bogdan, *Aerial Manipulation*. Cham, Switzerland: Springer International Publishing, 2018.

[4] M. Tognon, H. A. Tello Chávez, E. Gasparin, Q. Sablé, D. Bicego, A. Mallet, M. Lany, G. Santi, B. Revaz, J. Cortés, and A. Franchi, "A truly redundant aerial manipulator system with application to push-and-slide inspection in industrial plants," *IEEE Robotics and Automation Letters*, vol. 4, no. 2, pp. 1846–1851, 2019.

[5] C. D. Bellicoso, L. R. Buonocore, V. Lippiello, and B. Siciliano, "Design, modeling and control of a 5-DoF light-weight robot arm for aerial manipulation," in *2015 23rd Mediterranean Conf. Control and Automation (MED)*, June 2015, pp. 853–858.

[6] G. Heredia, A. E. Jimenez-Cano, I. Sanchez, D. Llorente, V. Vega, J. Braga, J. A. Acosta, and A. Ollero, "Control of a multirotor outdoor aerial manipulator," in *2014 IEEE/RSJ Int. Conf. Intelligent Robots and Systems*, Sept. 2014, pp. 3417–3422.

[7] M. Fumagalli, R. Naldi, A. Macchelli, F. Forte, A. Q. Keemink, S. Stramigioli, R. Carloni, and L. Marconi, "Developing an aerial manipulator prototype: Physical interaction with the environment," *IEEE Robotics & Automation Magazine*, vol. 21, no. 3, pp. 41–50, 2014.

[8] M. Tognon, B. Yüksel, G. Buondonno, and A. Franchi, "Dynamic decentralized control for protocentric aerial manipulators," in *2017 IEEE Int. Conf. Robotics and Automation (ICRA)*, 2017, pp. 6375–6380.

[9] D. Mellinger, Q. Lindsey, M. Shomin, and V. Kumar, "Design, modeling, estimation and control for aerial grasping and manipulation," in *2011 IEEE/RSJ Int. Conf. Intelligent Robots and Systems*, Sept. 2011, pp. 2668–2673, iSSN: 2153-0866.

[10] S. Hamaza and M. Kovac, "Omni-Drone: on the Design of a Novel Aerial Manipulator with Omni-directional Workspace," in *2020 17th Int. Conf. Ubiquitous Robots (UR)*, June 2020, pp. 153–158, iSSN: 2325-033X.

[11] M. Hamandi, F. Usai, Q. Sablé, N. Staub, M. Tognon, and A. Franchi, "Design of multirotor aerial vehicles: a taxonomy based on input allocation," *Int. Journal Robotics Research*, vol. 40, pp. 1015–1044, 2021/05 2021.

[12] S. Park, J. Lee, J. Ahn, M. Kim, J. Her, G.-H. Yang, and D. Lee, "Odar: Aerial manipulation platform enabling omnidirectional wrench generation," *IEEE/ASME Transactions on Mechatronics*, vol. 23, no. 4, pp. 1907–1918, 2018.

[13] D. Brescianini and R. D'Andrea, "An omni-directional multirotor vehicle," *Mechatronics*, vol. 55, pp. 76–93, 2018. [Online]. Available: https://www.sciencedirect.com/science/article/pii/S0957415818301314

[14] M. Kamel, S. Verling, O. Elkhatib, C. Sprecher, P. Wulkop, Z. Taylor, R. Siegwart, and I. Gilitschenski, "The voliro omniorientational hexacopter: An agile and maneuverable tiltable-rotor aerial vehicle," *IEEE Robotic and Automation Magazine*, vol. 25, no. 4, pp. 34–44, dec 2018.

[15] K. Bodie, Z. Taylor, M. Kamel, and R. Siegwart, "Towards efficient full pose omnidirectionality with overactuated MAVs," in *Springer Proceedings in Advanced Robotics*. Springer International Publishing, 2020, pp. 85–95. [Online]. Available: https://doi.org/10.1007/978-3-030-33950-0_8

[16] K. Bodie, M. Tognon, and R. Siegwart, "Dynamic end effector tracking with an omnidirectional parallel aerial manipulator," *IEEE Robotics and Automation Letters*, vol. 6, no. 4, pp. 8165–8172, 2021.

[17] C. Papachristos, K. Alexis, and A. Tzes, "Towards a high-end unmanned tri-tiltrotor: design, modeling and hover control," in *2012 20th Mediterranean Conf. Control Automation (MED)*, 2012, pp. 1579–1584.

[18] S. Lynen, M. W. Achtelik, S. Weiss, M. Chli, and R. Siegwart, "A robust and modular multi-sensor fusion approach applied to MAV navigation," in *2013 IEEE/RSJ Int. Conf. Intelligent Robots and Systems*. Tokyo: IEEE, Nov. 2013, pp. 3923–3929. [Online]. Available: http://ieeexplore.ieee.org/document/6696917/